Cyclic three-level-pulse-area theorem for enantioselective state transfer of chiral molecules

Yu Guo,[1,2,3] Xun Gong,[2] Songshan Ma,[1] and Chuan-Cun Shu (束传存)[1,*]

[1]*Hunan Key Laboratory of Nanophotonics and Devices, School of Physics and Electronics, Central South University, Changsha 410083, China*

[2]*Hunan Provincial Key Laboratory of Flexible Electronic Materials Genome Engineering, School of Physics and Electronic Science, Changsha University of Science and Technology, Changsha 410114, China*

[3]*Key Laboratory of Low-Dimensional Quantum Structures and Quantum Control of Ministry of Education, Hunan Normal University, Changsha 410081, China*

(Received 1 September 2021; accepted 15 December 2021; published 3 January 2022)

We derive a pulse-area theorem for a single-loop cyclic three-level system without applying the rotating-wave approximation while explicitly taking into account the time delays of control fields. This corresponds to an archetypal model for exploring enantioselective state transfer (ESST) in chiral molecules driven by three linearly polarized microwave pulses. By dividing the closed-loop excitation into two separate stages, we obtain both amplitude and phase conditions of three control fields to generate high fidelity of ESST. As a proof of principle, we apply this pulse-area theorem to cyclohexylmethanol molecules, for which three rotational states are connected by *a*-type, *b*-type, and *c*-type components of the transition dipole moments in both center-frequency-resonant and -detuned conditions. Our results show that two enantiomers with opposite handedness can be transferred to different target states by designing three microwave pulses that satisfy the amplitude and phase conditions at the transition frequencies. The corresponding control schemes are robust against the time delays between the two stages. We suggest that the two control fields used in the second stage should be applied simultaneously for practical applications. This work contributes an alternative pulse-area theorem to the field of quantum control, which has the potential to determine the chirality of enantiomers in a mixture.

DOI: 10.1103/PhysRevA.105.013102

I. INTRODUCTION

Since Pasteur first reported molecular chirality [1], the theoretical and experimental study of chiral molecules has drawn increasing interest because of its fundamental importance in modern chemical and biochemical industries as well as quantum science [2–5]. Two enantiomers of chiral molecules with opposite handedness have the same components and configuration for spatial reflection. This implies that distinguishing enantiomers from each other, highly related to the discrimination, separation, and purification of chiral molecules, remains a formidable task, because general physical properties of chiral molecules, such as boiling points, melting points, and densities, are the same for opposite enantiomers. Based on chemical mechanisms and enantiomer-specific interactions with auxiliary substances, many spectroscopic techniques were established to detect enantiomers of chiral molecules with different handedness [6–9]. Traditional chemical techniques, such as crystallization and chiral chromatography, are usually complicated and expensive because they require significantly longer than seconds or chirally pure derivatization reagents. In addition, previous theoretical works have shown that the interparticle interactions mediated by a bridging molecule via either the dispersion force [10–12] or resonant energy transfer [13–15] depend on the handedness of two enantiomers, making it possible to measure the chiral contributions.

By taking advantage of the sign difference property of rotational transition dipoles of two enantiomers, it has become promising to select enantiomers by designing coherent chiral control schemes [16–35]. The concept of adiabatic passage techniques, such as stimulated Raman adiabatic passages [36,37] and shortcuts to adiabaticity [38,39], was proposed to generate efficient and robust detection and separation of chiral molecules [40–45]. In order to meet adiabatic criteria, the adiabatic passage techniques involve strict limitations on the control fields and therefore the corresponding control processes are usually slow and complicated. To that end, nonadiabatic schemes using much shorter durations of control pulses than the adiabatic approaches have been proposed to reach fast enantioselective excitation of chiral molecules [46]. Experimentally, it has been demonstrated by using resonant microwave three-wave-mixing (M3WM) techniques [47–54]. A common feature of both adiabatic and nonadiabatic control schemes usually involves a closed-loop quantum system by cyclic coupling of three molecular (i.e., rotational or rovibrational) states (as shown in Fig. 1), which are resonantly driven through the *a*-type, *b*-type, and *c*-type components of the transition dipole moments by a combination of three orthogonally polarized and phase-controlled microwave fields [55]. Since one of three cyclic couplings differs in the sign of the transition dipole moment in two opposite enantiomers, the direct one-photon transition path from the ground state

*cc.shu@csu.edu.cn he/him/his

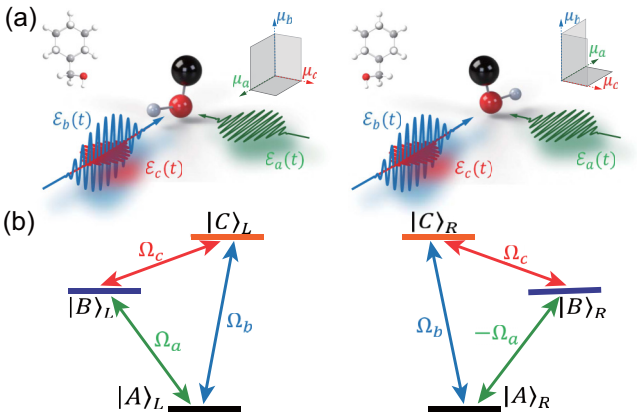

FIG. 1. Schematic illustration of enantioselective state transfer. (a) Space orientations of the dipole components $\mu_{a,b,c}$ in the molecule-fixed coordinate with respect to the polarization directions of three linearly polarized microwave pulses $\mathcal{E}_{a,b,c}(t)$. (b) Corresponding closed-loop transitions within three rotational states $|A\rangle$, $|B\rangle$, and $|C\rangle$. The transition frequencies and couplings between states are identical, except for a difference due to the sign difference in the transition dipole moment μ_{AB}. The parameters of the cyclohexylmethanol molecules are used for numerical simulations

to a given target state constructively or destructively interferes with the indirect two-photon transition path through an intermediate state, leading to enantioselective state transfer (ESST). Although the pulse areas of the three control fields that can generate enantioselective excitation have been experimentally examined in M3WM experiments, a general pulse-area theorem that can be used to directly calculate the amplitudes and phases of three time-dependent control pulses so as to gain insight into the underlying coherent quantum control mechanism is still lacking.

In this paper we focus on ESST and present a three-level-pulse-area theorem analysis. Previous works derived the pulse-area theorems for two-level systems [56,57] and three-level quantum systems with ladder-, Λ-, and V-type configurations [58–61], leading to many successful applications in coherent quantum control simulations and experiments [62–67]. Note that the pulse-area theorem of a two-level model under resonant and off-resonant conditions with the rotating-wave approximation has been investigated for controlling the populations of the left- versus right-handed excited states of enantiomers by using circularly polarized lights [68–70]. Here we take the strategy of dividing the closed-loop three-level excitation into two separate stages, i.e., combining a two-level excitation and a time-delayed open-loop three-level transition. We derive a pulse-area theorem of the three-level system with a Δ-type configuration without applying the rotating-wave approximation while explicitly taking into account the time delays of the laser pulses in coherent chiral control schemes. The derived pulse-area theorem can calculate the exact amplitude and phase conditions for generating efficient ESST to the desired quantum state, which is examined in cyclohexylmethanol molecules with different pulse sequences. This work provides an essential reference for coherent control of ESST using closed-loop three-level interaction schemes.

The remainder of this paper is organized as follows. In Sec. II we describe the theoretical methods for obtaining a three-level-pulse-area theorem with cyclic coupling. We perform numerical simulations to examine the derived pulse-area theorem in Sec. III. We conclude with a summary in Sec. IV.

II. THEORETICAL METHOD AND NUMERICAL MODEL

A. Closed-loop three-level model

To describe our model, three rotational states of asymmetric top molecules, as shown in Fig. 1, are labeled as $|A\rangle$, $|B\rangle$, and $|C\rangle$ with a subscript L (R) for the left- (right-)handed enantiomer, which can be expressed as superpositions of symmetric top eigenstates (see details in Refs. [54,55]). The energies E_A, E_B, and E_C of three rotational states are identical for enantiomers. We mark three microwave control fields as $\mathcal{E}_{a,b,c}(t)$, which drive the three states with the dipole moments $\mu^{L\,(R)}$ consisting of three components $\hat{\mu}_a$, $\hat{\mu}_b$, and $\hat{\mu_c}$ in the molecule-fixed coordinate. The triple product $\hat{\mu}_a \cdot (\hat{\mu}_b \times \hat{\mu}_c)$ is independent of the choice of the inertia principal axes a, b, and c, but is of opposite sign for the left- and right-handed enantiomers. As demonstrated in Refs. [55,71], the ESST scheme with the use of linearly polarized control fields requires a combination of fields $\mathcal{E}_a$, $\mathcal{E}_b$, and $\mathcal{E}_c$ with three orthogonal polarization directions in the space-fixed coordinate. The molecule-fixed coordinate is related to the space-fixed coordinate by the Euler angles (θ, ϕ, and χ). To that end, we describe the time- and polarization-dependent electric fields of the three control fields by

$$\mathcal{E}_{a,b,c}(t) = \mathbf{e}_{a,b,c}\mathcal{E}_{a,b,c}f_{a,b,c}(t)\cos[\omega_{a,b,c}(t - t_{a,b,c}) + \phi_{a,b,c}], \tag{1}$$

where $\mathbf{e}_{a,b,c}$, $\mathcal{E}_{a,b,c}$, $f_{a,b,c}(t)$, $\omega_{a,b,c}$, $t_{a,b,c}$, and $\phi_{a,b,c}$ denote the polarization direction, strength, envelope function, center frequency, center time, and phase of $\mathcal{E}_{a,b,c}(t)$, respectively. The Hamiltonian of the two different handed enantiomers driven by the control fields in the energy basis can be written as ($\hbar = 1$)

$$H^{L,R}(t) = \begin{pmatrix} E_A & \pm\Omega_a(t) & \Omega_b(t) \\ \pm\Omega_a(t) & E_B & \Omega_c(t) \\ \Omega_b(t) & \Omega_c(t) & E_C \end{pmatrix}, \tag{2}$$

where the three cyclic couplings read $\Omega_a(t) = -|\langle A|\hat{\mu}^{L\,(R)} \cdot \mathbf{e}_a|B\rangle|\mathcal{E}(t) = -|\mu_{AB}|\mathcal{E}_a(t)$, $\Omega_b(t) = -\langle A|\hat{\mu}^{L\,(R)} \cdot \mathbf{e}_b|C\rangle\mathcal{E}_b(t) = -\mu_{AC}\mathcal{E}_b(t)$, and $\Omega_c(t) = -\langle B|\hat{\mu}^{L\,(R)} \cdot \mathbf{e}_c|C\rangle\mathcal{E}_c(t) = -\mu_{BC}\mathcal{E}_c(t)$. In this work we specify that the transition dipole moments μ_{AC} and μ_{BC} are identical for two enantiomers, whereas the transition dipole moment μ_{AB} changes sign with the handedness reflected in Eq. (2) by the sign $\pm$. The evolution of the three states can be described by using the time-dependent wave function $|\psi(t)\rangle = \sum_{X=A,B,C} C_X(t)\exp(-iE_X t)|X\rangle$ with the complex coefficients $C_X(t)$.

We now analyze how to achieve enantioselective excitation of a given target state from a given initial state. We assume that two enantiomers are initially in the state $|A\rangle$, and the control target can be either the excited state $|B\rangle$ or $|C\rangle$. For the choice of $|C\rangle$ as the target, there are a direct one-photon transition $|A\rangle \leftrightarrow |C\rangle$ and an indirect two-photon transition $|A\rangle \leftrightarrow$

$|B\rangle \leftrightarrow |C\rangle$, which form the closed-loop interaction scheme. If we take $|B\rangle$ as the target, two transition paths correspond to a direct one $|A\rangle \leftrightarrow |B\rangle$ and an indirect one $|A\rangle \leftrightarrow |C\rangle \leftrightarrow |B\rangle$. Since it remains difficult to derive an analytical solution by directly using the Hamiltonian in Eq. (2), we use the strategy of dividing the excitation processes into two stages.

B. Control conditions for ESST to $|C\rangle$

1. Analytical solution for a two-level system

For the ESST to $|C\rangle$, we assume that the coupling Ω_a is turned on at the initial time t_0 and off at a time t_1 before the couplings Ω_b and Ω_c. Thus, the system is reduced to a two-level system and the corresponding Hamiltonian reads

$$H_1^{L,R}(t) = \begin{pmatrix} E_A & \pm\Omega_a(t) \\ \pm\Omega_a(t) & E_B \end{pmatrix}. \tag{3}$$

Without using the rotating-wave approximation, the evolution of the system in the interaction picture can be described by using the unitary operator

$$U_1^{L,R}(t,t_0) = U_1^{L,R}(t_0,t_0) - i\int_{t_0}^{t} dt' H_{1I}^{L,R}(t') U_1^{L,R}(t',t_0), \tag{4}$$

where $H_{1I}^{L,R}(t) = \exp(iH_{10}t)[\pm\Omega_a(t)(|A\rangle\langle B| + |B\rangle\langle A|)]\exp(-iH_{10}t)$ with the field-free Hamiltonian of the two-level system $H_{10} = E_A|A\rangle\langle A| + E_B|B\rangle\langle B|$. By involving the first-order Magnus expansion [72], the time-dependent unitary operator $U_1^{L,R}(t,t_0)$ can be given by [60,61,64,65]

$$\begin{aligned} U_1^{L,R}(t,t_0) &= \cos|\theta_a(t)|(|A\rangle\langle A| + |B\rangle\langle B|) \\ &\quad \mp i\sin|\theta_a(t)|\left[\frac{|\theta_a(t)|}{\theta_a^*(t)}|B\rangle\langle A| + \frac{|\theta_a(t)|}{\theta_a(t)}|A\rangle\langle B|\right] \end{aligned} \tag{5}$$

in terms of the complex pulse area $\theta_a(t) = \int_{t_0}^{t}\Omega_a(t')\exp(i\omega_{AB}t')dt'$, with $\omega_{AB} = E_B - E_A$. By considering the left- and right-handed enantiomers initially in the ground state $|A\rangle$, an analytic solution for the wave function of the two-level system can be obtained by

$$\begin{aligned} |\psi_1^{L,R}(t)\rangle &= U_1^{L,R}(t,t_0)|A\rangle \\ &= \cos|\theta_a(t)||A\rangle \mp i\frac{|\theta_a(t)|}{\theta_a^*(t)}\sin|\theta_a(t)||B\rangle. \end{aligned} \tag{6}$$

2. Analytical solution for a three-level system

After the coupling Ω_a off at t_1, we turn on the couplings Ω_b and Ω_c. The Hamiltonian in Eq. (2) is reduced to

$$H_2^{L,R}(t) = \begin{pmatrix} E_A & 0 & \Omega_b(t) \\ 0 & E_B & \Omega_c(t) \\ \Omega_b(t) & \Omega_c(t) & E_C \end{pmatrix}. \tag{7}$$

The corresponding time-dependent unitary operator can be given by

$$U_2^{L,R}(t,t_1) = U_2^{L,R}(t_1,t_1) - i\int_{t_1}^{t} dt' H_{2I}^{L,R}(t') U_2^{L,R}(t',t_1), \tag{8}$$

where $H_{2I}^{L,R}(t) = \exp(iH_{20}t)[\Omega_b(t)(|A\rangle\langle C| + |C\rangle\langle C|) + \Omega_c(t)(|C\rangle\langle B| + |B\rangle\langle C|)]\exp(-iH_{20}t)$, with the field-free Hamiltonian of the three-level system $H_{20} = E_A|A\rangle\langle A| + E_B|B\rangle\langle B| + E_C|C\rangle\langle C|$. By making the first-order Magnus expansion of the unitary operator $U_2^{L,R}(t,t_1)$, the time-dependent wave function of two enantiomers can be given by

$$\begin{aligned} |\psi_2^{L,R}(t)\rangle = U_2^{L,R}(t,t_1)|\psi_1^{L,R}(t_1)\rangle &= \left[\cos|\theta_a(t_1)|\frac{|\theta_c(t)|^2 + |\theta_b(t)|^2\cos\theta(t)}{\theta^2(t)} \mp i\sin|\theta_a(t_1)|\zeta(t)\frac{|\theta_a(t_1)|}{\theta_a^*(t_1)}\right]|A\rangle \\ &+ \left[\cos|\theta_a(t_1)|\zeta^*(t) \mp i\sin|\theta_a(t_1)|\frac{|\theta_a(t_1)|}{\theta_a^*(t_1)}\frac{|\theta_b(t)|^2 + |\theta_c(t)|^2\cos\theta(t)}{\theta^2(t)}\right]|B\rangle \\ &- \frac{\sin\theta(t)}{\theta(t)}\left[i\cos|\theta_a(t_1)|\theta_b(t) \pm \sin|\theta_a(t_1)|\theta_c(t)\frac{|\theta_a(t_1)|}{\theta_a^*(t_1)}\right]|C\rangle, \end{aligned} \tag{9}$$

where $\zeta(t) = \theta_c(t)\theta_b^*(t)[\cos\theta(t) - 1]/\theta^2(t)$ and $\theta(t) = \sqrt{|\theta_b(t)|^2 + |\theta_c(t)|^2}$ in terms of the complex pulse areas $\theta_b(t) = \int_{t_1}^{t}\Omega_b(t')\exp(i\omega_{AC}t')dt'$ and $\theta_c(t) = \int_{t_1}^{t}\Omega_c(t')\exp(i\omega_{BC}t')dt'$, with the transition frequencies $\omega_{BC} = E_C - E_B$ and $\omega_{AC} = E_C - E_A$.

To entirely transfer the left-handed enantiomer to the state $|C\rangle$ while keeping the right-handed one unpopulated at the final time t_f, the complex pulse areas should satisfy the two relations

$$\left|\frac{\sin\theta(t_f)}{\theta(t_f)}\left[i\theta_b(t_f)\cos|\theta_a(t_1)| + \frac{|\theta_a(t_1)|\theta_c(t_f)}{\theta_a^*(t_1)}\sin|\theta_a(t_1)|\right]\right| = 1, \tag{10}$$

$$\left|\frac{\sin\theta(t_f)}{\theta(t_f)}\left[i\theta_b(t_f)\cos|\theta_a(t_1)| - \frac{|\theta_a(t_1)|\theta_c(t_f)}{\theta_a^*(t_1)}\sin|\theta_a(t_1)|\right]\right| = 0. \tag{11}$$

From the Eq. (11) we can derive

$$\frac{\theta_c(t_f)}{\theta_a^*(t_1)} = \frac{i\theta_b(t_f)\cos|\theta_a(t_1)|}{|\theta_a(t_1)|\sin|\theta_a(t_1)|}. \tag{12}$$

By inserting Eq. (12) into Eq. (10), we can obtain the relation

$$4|\theta_b(t_f)|^2 \sin^2\theta(t_f)\cos^2|\theta_a(t_1)| = \theta^2(t_f). \tag{13}$$

This relation can be fulfilled when the three control fields satisfy the amplitude conditions

$$|\theta_b(t_f)| = |\theta_c(t_f)| = \frac{1}{\sqrt{2}}\left(k+\frac{1}{2}\right)\pi \quad (k \in N),$$
$$|\theta_a(t_1)| = \left(k'+\frac{1}{4}\right)\pi \quad (k' \in N). \tag{14}$$

Furthermore, we insert Eq. (14) into Eq. (12) with $\theta_b = -|\theta_b|\exp[-i(\phi_b - \omega_{AC}t_b)]$, $\theta_c = -|\theta_c|\exp[-i(\phi_c - \omega_{BC}t_c)]$, and $\theta_a = -|\theta_a|\exp[-i(\phi_a - \omega_{AB}t_a)]$. We find that the three control fields satisfy the phase condition

$$\phi_a + \phi_c - \phi_b = \left(2l+\tfrac{1}{2}\right)\pi + (\omega_{AB}t_a + \omega_{BC}t_c - \omega_{AC}t_b) \quad (l \in Z). \tag{15}$$

Similarly, we can use the same amplitude conditions as those in Eq. (14) to achieve complete ESST to $|C\rangle$ of the right-handed enantiomer by using the phase condition of $\phi_a + \phi_c - \phi_b = (2l - \frac{1}{2})\pi + (\omega_{AB}t_a + \omega_{BC}t_c - \omega_{AC}t_b)$ $(l \in Z)$. This implies that a π flip of the phase on one of three control fields can result in the opposite ESST. To that end, the handedness of enantiomers can be determined by measuring the population in the state $|C\rangle$.

C. Control conditions for ESST to $|B\rangle$

For ESST to $|B\rangle$, we apply the coupling Ω_b before the couplings Ω_a and Ω_c, which results in a coherent superposition state of $|A\rangle$ and $|C\rangle$. As demonstrated above by involving the first-order Magnus expansion and further mathematical derivations, an analytic wave function of the three-level Λ-type system can be given by

$$\begin{aligned}\left|\psi_2^{L,R}(t)\right\rangle = &\left[\cos|\theta_b(t_1)|\frac{|\theta_c(t)|^2 + |\theta_a(t)|^2\cos\theta(t)}{\theta^2} \mp i\sin|\theta_b(t_1)|\xi^*(t)\frac{|\theta_b(t_1)|}{\theta_b^*(t_1)}\right]|A\rangle \\ &- \frac{\sin\theta(t)}{\theta(t)}\left[\sin|\theta_b(t_1)|\theta_c^*(t)\frac{|\theta_b(t_1)|}{\theta_b^*(t_1)} \pm i\cos|\theta_b(t_1)|\theta_a(t)\right]|B\rangle \\ &- \left[i\sin|\theta_b(t_1)|\frac{|\theta_b(t_1)|}{\theta_b^*(t_1)}\frac{|\theta_a(t)|^2 + |\theta_c(t)|^2\cos\theta(t)}{\theta^2(t)} \mp \cos|\theta_b(t_1)|\xi(t)\right]|C\rangle,\end{aligned} \tag{16}$$

where $\xi(t) = \theta_c(t)\theta_a(t)[\cos\theta(t) - 1]/\theta^2(t)$ and $\theta(t) = \sqrt{|\theta_a(t)|^2 + |\theta_c(t)|^2}$.

To entirely transfer the left-handed enantiomer to the state $|B\rangle$ at the final time t_f, but with the right-handed one not populating, we have

$$\left|\frac{\sin\theta(t_f)}{\theta(t_f)}\left[\sin|\theta_b(t_1)|\theta_c^*(t_f)\frac{|\theta_b(t_1)|}{\theta_b^*(t_1)} + i\cos|\theta_b(t_1)|\theta_a(t_f)\right]\right| = 1, \tag{17}$$

$$\left|\frac{\sin\theta(t_f)}{\theta(t_f)}\left[\sin|\theta_b(t_1)|\theta_c^*(t_f)\frac{|\theta_b(t_1)|}{\theta_b^*(t_1)} - i\cos|\theta_b(t_1)|\theta_a(t_f)\right]\right| = 0. \tag{18}$$

Furthermore, we can obtain the amplitude condition for the three control fields

$$|\theta_a(t_f)| = |\theta_c(t_f)| = \frac{1}{\sqrt{2}}\left(k+\frac{1}{2}\right)\pi \quad (k \in N),$$
$$|\theta_b(t_1)| = \left(k'+\frac{1}{4}\right)\pi \quad (k' \in N). \tag{19}$$

The ESST to $|B\rangle$ of the left-handed enantiomer can be reached by using the phase condition

$$\phi_a + \phi_c - \phi_b = \left(2l-\tfrac{1}{2}\right)\pi + (\omega_{AB}t_a + \omega_{BC}t_c - \omega_{AC}t_b) \quad (l \in Z). \tag{20}$$

The amplitude conditions in Eq. (19) are of the same form as Eq. (13) with different orders. That is, the orders of the three pulses are interchangeable, dependent on the choice of the target state. From the phase condition in Eq. (20), we can find that a π flip of the phase on one of three control fields can also lead to the opposite ESST. Since our schemes that divide the closed-loop excitation schemes into two stages are different from previous works [27–29,45,52], which turned on the direct one-photon transition path before the two-photon one, these amplitude and phase conditions provide an alternative way to achieve ESST within a cyclic three-level system in chiral molecules. In addition, we find that our derived phase conditions in Eqs. (15) and (20) explicitly include time delays $t_{a,b,c}$, indicating that the time delays of the second stage play important roles in achieving the ESST.

Note that the amplitude conditions of $|\theta_{a,b}(t_f)| = \pi/4$ and $|\theta(t_f)| = \sqrt{|\theta_{b,a}(t_f)|^2 + |\theta_c(t_f)|^2} = \pi/2$ are equivalent to those with the use of $\pi/2$ and π pulses, for which a scale of $\frac{1}{2}$ factor comes from the definition of the complex pulse areas without using the rotating-wave approximation and the resonant excitation conditions. To show the advantage of using the complex pulse areas, we can have a frequency-domain analysis for the control fields

$$\mathcal{E}_{a,b,c} = \frac{1}{\pi}\int_{t_0}^{t_f} d\omega\, \mathcal{A}_{a,b,c}(\omega)e^{i\phi_{a,b,c}(\omega)}e^{i\omega t}, \tag{21}$$

where $\mathcal{A}_{a,b,c}(\omega)$ and $\phi_{a,b,c}(\omega)$ are the spectral amplitude and phase, respectively. We find that the values of $\theta_{a,b,c}(t_f)$ depend only on $\mathcal{A}_{a,b,c}(\omega)$ and $\phi_{a,b,c}(\omega)$ of three control fields at transition frequencies ω_{AB}, ω_{AC}, and ω_{BC}. Thus, our definitions of the complex pulse areas can also be applied to the pulsed control fields whose center frequencies are detuned away from the transition frequencies. In Sec. III we present simulations to examine the amplitude and phase conditions for both center-frequency-resonant and -detuned microwave excitation schemes.

III. RESULTS AND DISCUSSION

We perform numerical simulations for the cyclohexylmethanol molecules. Three rotational states of $|1_{01}\rangle$, $|2_{02}\rangle$, and $|2_{12}\rangle$ are used as $|A\rangle$, $|B\rangle$, and $|C\rangle$. The transition frequencies between states are $\omega_{AB} = 4720$ MHz, $\omega_{BC} = 2339$ MHz, and $\omega_{AC} = 7059$ MHz and the transition dipole moments take the values $\mu_a = 0.4$ D, $\mu_b = 1.2$ D, and $\mu_c = 0.8$ D [27,54]. In our simulations, we take three control fields with the Gaussian profile as

$$\mathcal{E}_{a,b,c}(t) = \sqrt{\frac{2}{\pi}}\frac{A_{a,b,c}}{\tau_0}\exp\left[-\frac{(t-t_{a,b,c})^2}{2\tau_0^2}\right] \times \cos[\omega_{a,b,c}(t-t_{a,b,c})+\phi_{a,b,c}]. \quad (22)$$

This description of the control fields is convenient for determining the field strengths $\mathcal{E}_{a,b,c}$ for any accessible duration τ_0. By choosing constant values of $A_{a,b,c}$, we can see that the complex pulse areas $\theta_{a,b,c}(t_f)$ with such descriptions do not depend on the duration τ_0. Thus, this scheme avoids the strict limitations by the adiabatic criterion, providing a way to design fast control schemes using much shorter pulse duration than the adiabatic scenario. For practical applications, however, we need to balance the choice of pulse duration τ_0 so that unwanted transitions to neighboring energy levels could be avoided by using narrowband pulses.

For cyclohexylmethanol molecules, there exists a rotational state $|1_{11}\rangle$ with energy slightly below state $|B\rangle$, referred to as state $|B'\rangle$, which can be connected to the excited state $|C\rangle$ via the a-type transition in $\omega_{B'C} = 4484$ MHz and to the ground state $|A\rangle$ via the c-type transition in $\omega_{AB'} = 2575$ MHz. To this end, we include it in a four-level model to perform the numerical simulations and examine how to choose the laser pulses to exclude the effect of this state in the ESST so that the system can be reduced to the three-level model developed above. The corresponding field-molecule interaction Hamiltonian reads

$$H_c^{L,R}(t) = \begin{pmatrix} 0 & \Omega_c'(t) & \pm\Omega_a(t) & \Omega_b(t) \\ \Omega_c'(t) & 0 & 0 & \pm\Omega_a'(t) \\ \pm\Omega_a(t) & 0 & 0 & \Omega_c(t) \\ \Omega_b(t) & \pm\Omega_a'(t) & \Omega_c(t) & 0 \end{pmatrix}, \quad (23)$$

where we use the additional couplings $\Omega_a'(t) = -\langle B'|\hat{\mu}\cdot\mathbf{e}_a|C\rangle\mathcal{E}_a(t) = -\mu_{B'C}\mathcal{E}_a(t)$ and $\Omega_c'(t) - \langle A|\hat{\mu}\cdot\mathbf{e}_c|B'\rangle\mathcal{E}_c(t) = -\mu_{AB'}\mathcal{E}_c(t)$ in our simulations. The time-dependent unitary operator in the interaction picture can be numerically computed by

$$U^{L,R}(t,t_0) = U^{L,R}(t_0,t_0) - i\int_{t_0}^{t} dt' H_I^{L,R}(t')U^{L,R}(t',t_0), \quad (24)$$

where $U^{L,R}(t_0,t_0) = \mathbb{I}$ and $H_I^{L,R}(t) = \exp(iH_0t)[H_c^{L,R}(t)]\exp(-iH_0t)$ with the field-free Hamiltonian $H_0 = \sum_{X=A}^{C} E_X|X\rangle\langle X|$. By projecting the unitary operator $U^{L,R}(t,t_0)$ onto the initial state $|A\rangle$, we can obtain the time-dependent wave function of the system $|\psi^{L,R}(t)\rangle = U^{L,R}(t,t_0)|A\rangle$ without using the first-order Magnus expansion. Thus, the time-dependent population in the state $|X\rangle$ can be calculated by $P_X^{L,R}(t) = |\langle X|\psi^{L,R}(t)\rangle|^2$ with $X = A, B', B, C$.

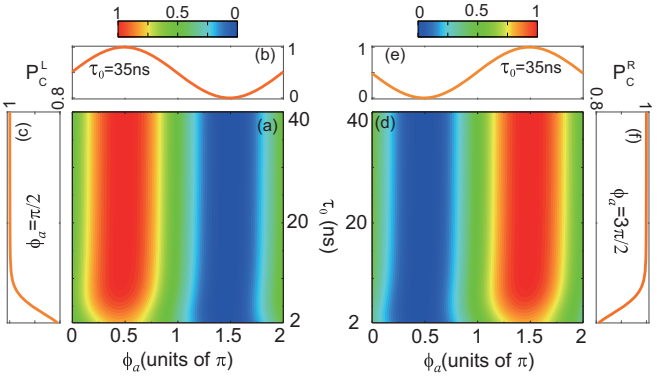

FIG. 2. Chiral dependence of ESST on the phase for the target state $|C\rangle$. (a) Final population of the left-handed enantiomer $P_C^L(t_f)$ versus the duration τ_0 and phase ϕ_a in a range of $[0, 2\pi]$ and the corresponding cut lines at (b) $\tau_0 = 35$ ns and (c) $\phi_a = \pi/2$. (d)–(f) Same as (a)–(c) for the right-handed enantiomer except for $\phi_a = 3\pi/2$ in (f). The parameters are chosen with $\phi_b = \phi_c = 0$ while setting $t_a = 4\tau_0$ and $t_b = t_c$ at a value to satisfy Eq. (15).

A. ESST to $|C\rangle$

For the target state $|C\rangle$, we set the parameters $A_a = \pi/4\mu_{AB}$, $A_b = \pi/2\sqrt{2}\mu_{BC}$, and $A_c = \pi/2\sqrt{2}\mu_{AC}$. It is easy to verify that the couplings $\Omega_{a,b,c}(t)$ with the three control fields defined by Eq. (22) with different values of τ_0 exactly satisfy the amplitude conditions in Eq. (14) at transition frequencies by fixing the center frequencies $\omega_a = \omega_{AB}$, $\omega_b = \omega_{AC}$, and $\omega_c = \omega_{BC}$ and are independent of the values of the transition dipole moments of the system. Figure 2 shows the results of $P_C^{L,R}(t_f)$ versus τ_0 and ϕ_a with $\phi_b = \phi_c = 0$. As expected, the ESST to the state $|C\rangle$ appears and depends strongly on the phase values of ϕ_a. The fidelity of $P_C^{L,R}(t_f) > 0.999$ can be reached for $\tau_0 > 35$ ns, indicating that the unwanted transition to the neighboring state $|B'\rangle$ can be ignored. Figures 2(b) and 2(e) plot the dependence of $P_C^{L,R}(t_f)$ on the phase ϕ_a for the case of $\tau_0 = 35$ ns. There is no ESST at $\phi_a = 0$ and π. The entire ESST to the left-handed molecule occurs at $\phi_a = \pi/2$ and a phase change to $\phi_a = 3\pi/2$ results in an opposite transfer to the right-handed one. Similar features can be observed by changing the value of ϕ_b (ϕ_c) while choosing $\phi_a = \phi_c = 0$ ($\phi_a = \phi_b = 0$). These results are in good agreement with the theoretical predication by the phase conditions as well as previous M3WM experiments. To visualize the

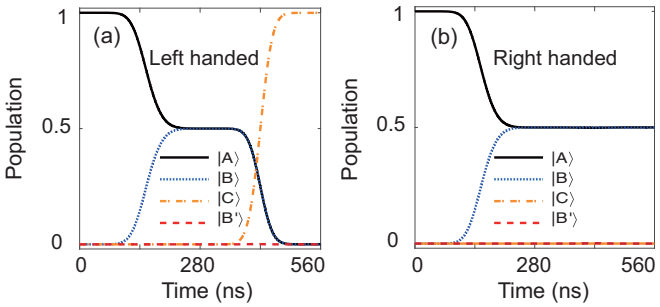

FIG. 3. Time-dependent populations of four rotational states for ESST to the state $|C\rangle$. Simulations for the (a) left-handed and (b) right-handed enantiomers with duration $\tau_0 = 35$ ns and phase $\phi_a = \pi/2$ are shown. The other parameters are chosen with $\phi_b = \phi_c = 0$ while setting $t_a = 4\tau_0$ and $t_b = t_c$ at a value to satisfy Eq. (15).

underlying quantum state transfer mechanism, Fig. 3 shows the time-dependent populations of the four states induced by the control fields for the cases of $\tau_0 = 35$ ns and $\phi_a = \pi/2$. For the two enantiomers, there are no visible populations in the state $|B'\rangle$ during the whole process. The four-level system is equivalent to the present closed-loop three-level model with the pulse parameters used. The control field $\mathcal{E}_a(t)$ with the pulse areas $\theta_a(t_1) = \pi/4$ drives the system to the maximal coherent superposition of $|A\rangle$ and $|B\rangle$ with $P_A^{L,R}(t_1) = P_B^{L,R}(t_1) = 0.5$ for both enantiomers. Due to the sign difference of the transition from $|A\rangle$ to $|B\rangle$, $\mathcal{E}_a(t)$ with a phase $\phi_a = \pi/2$ will result in the phase of the state $|B\rangle$ in 0 and π for the left and right handedness, respectively, as described by Eq. (9). For the left handedness, the transition path from $|A\rangle$ to $|C\rangle$ induced by $\mathcal{E}_b(t)$ will constructively interfere with the path from $|B\rangle$ to $|C\rangle$ by $\mathcal{E}_c(t)$, leading to a complete ESST to $|C\rangle$. For right handedness, however, the two paths are destructive, which keeps the molecules in the states $|A\rangle$ and $|C\rangle$, as shown in Figs. 3(a) and 3(b).

As can be seen from our theoretical derivations, we divide the closed-loop excitation scheme into two time-separated stages. To see whether the amplitude and phase conditions can be applied to the overlapped cases, as an example, Fig. 4 plots the landscape of $P_C^L(t_f)$ with respect to the time delays

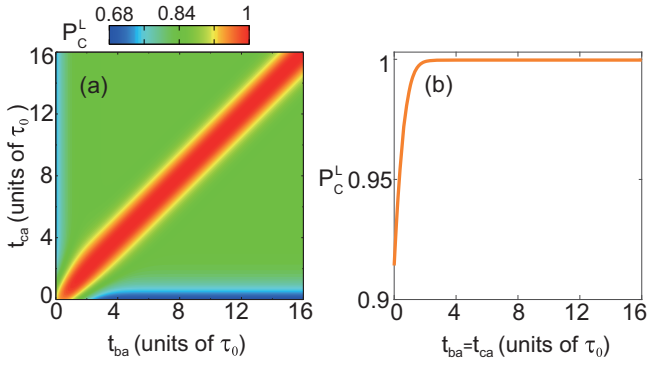

FIG. 4. Dependence of ESST on the time delays of control fields for the target state $|C\rangle$. (a) Final population of the left-handed enantiomer $P_C^L(t_f)$ versus the time delays $t_{ba} = t_b - t_a$ and $t_{ca} = t_c - t_a$. (b) Cut line plot of $P_C^L(t_f)$ along $t_{ba} = t_{ca}$.

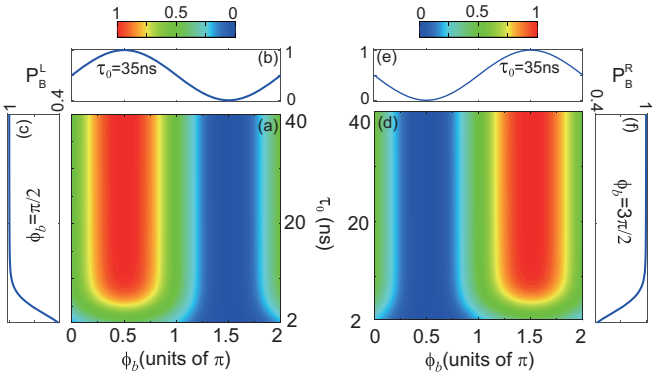

FIG. 5. Chiral dependence of ESST on the phase for the target state $|B\rangle$. (a) Final population of the left-handed enantiomer $P_C^L(t_f)$ versus the duration τ_0 and phase ϕ_b in a range of $[0, 2\pi]$ and the corresponding cut lines at (b) $\tau_0 = 35$ ns and (c) $\phi_b = \pi/2$. (d)–(f) Same as (a)–(c) for the right-handed enantiomer except for $\phi_a = 3\pi/2$ in (f). The other parameters are chosen with $\phi_a = \phi_c = 0$ while setting $t_b = 4\tau_0$ and $t_a = t_c$ at a value to satisfy Eq. (20).

$t_{ba} = t_b - t_a$ and $t_{ca} = t_c - t_a$ while keeping the center time t_a unchanged. In our simulations, we set $\phi_b = \phi_c = 0$ and $\phi_a = \pi/2 + (\omega_{AB}t_a + \omega_{BC}t_c - \omega_{AC}t_b)$ to satisfy Eq. (15). We find that $P_C^L(t_f)$ strongly depends on the overlap between two control fields of the second stage. Interestingly, the value of $P_C^L(t_f)$ remains $P_C^L(t_f) > 0.999$ for $t_{ba} = t_{ca} > 2\tau_0$ when $\mathcal{E}_b(t)$ and $\mathcal{E}_c(t)$ are turned on simultaneously with $t_{ba} = t_{ca}$. Even when the three control fields are applied without any delays, the high fidelity of $P_C^L(t_f) > 0.90$ holds, as shown in Fig. 4(b). This phenomenon can also be observed for the right handedness (not shown here).

B. ESST to $|B\rangle$

Figure 5 examines the same simulations as in Fig. 2 but for the target $|B\rangle$ with $\phi_a = \phi_c = 0$. In our simulations, we choose the parameters $A_b = \pi/4\mu_{BC}$, $A_a = \pi/2\sqrt{2}\mu_{AB}$, and $A_c = \pi/2\sqrt{2}\mu_{AC}$ so that all control fields satisfy the amplitude conditions. The influence of the state $|B'\rangle$ is more visible than that in Fig. 2 in the short-duration regime, which becomes rather weak with increasing duration τ_0. The final population $P_B^{L,R}(t_f)$ can also reach high fidelity for $\tau_0 > 35$ ns. As demonstrated in Fig. 2, the landscape of $P_B^{L,R}(t_f)$ exhibits a chiral symmetry with respect to the phase ϕ_b, for which the control field $\mathcal{E}_b(t)$ with $\phi_b = \pi/2$ leads to a complete ESST to $|B\rangle$ for the left handedness. For the right handedness, however, $\phi_b = 3\pi/2$ is required. This dependence of $P_B^{L,R}(t_f)$ on the phase is consistent with the theoretical predication. Figure 6 plots the time-dependent populations of the system with $\tau_0 = 35$ ns and $\phi_b = \pi/2$. Since the transition moments μ_b are identical for the two enantiomers without a difference of sign, $\mathcal{E}_b(t)$ plays the same role in the first stage, generating the same maximal coherent superposition of $|A\rangle$ and $|C\rangle$. The constructive or destructive interference that depends on μ_a occurs between the transition paths from $|A\rangle$ and $|C\rangle$ to $|B\rangle$. As a result, the left-handed enantiomer is fully transferred to the state $|B\rangle$, whereas the right-handed one is still in the coherent states $|A\rangle$ and $|B\rangle$ at end of three pulses. To see the

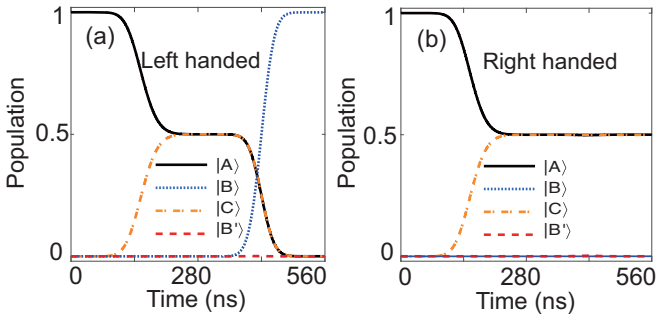

FIG. 6. Time-dependent populations of four rotational states for ESST to the state $|B\rangle$. Simulations for the (a) left-handed and (b) right-handed enantiomers with duration $\tau_0 = 35$ ns and phase $\phi_b = \pi/2$ are shown. The other parameters are chosen with $\phi_a = \phi_c = 0$ while setting $t_b = 4\tau_0$ and $t_a = t_c$ at a value to satisfy Eq. (20).

robustness of the scheme on the time delays, Fig. 7 examines the dependence of $P_B^L(t_f)$ on the time delays $t_{ab} = t_a - t_b$ and $t_{cb} = t_c - t_b$. In this simulation, we set $\phi_a = \phi_c = 0$ and $\phi_b = \pi/2 + (\omega_{AB}t_a + \omega_{BC}t_c - \omega_{AC}t_b)$ to satisfy the phase condition in Eq. (20). Similar behaviors can be observed, indicating that both excitation schemes do not require strict separations between the control fields. The identical delays of the second stage fields are beneficial for the control. As a result, the amplitude and phase conditions can also be used for the overlapping control fields, leading to the high selectivity of handedness.

C. ESST with center-frequency-detuned pulses

Finally, we examine the amplitude and phase conditions of control fields whose center frequencies $\omega_{a,b,c}$ are not exactly resonant with the transition center frequencies ω_{AB}, ω_{BC}, and ω_{AC}. As can be seen from the definitions of the complex pulse areas $\theta_{a,b,c}(t_f)$, when the center frequencies are detuned away from resonances, the values of $|\theta_{a,b,c}(t_f)|$ will decrease while the parameters $A_{a,b,c}$ remain the same as those used in resonant cases. We can increase the values of $A_{a,b,c}$ to increase the values of $\theta_{a,b,c}(t_f)$ at the transition frequencies so as to satisfy the amplitude conditions. That is, the ESST

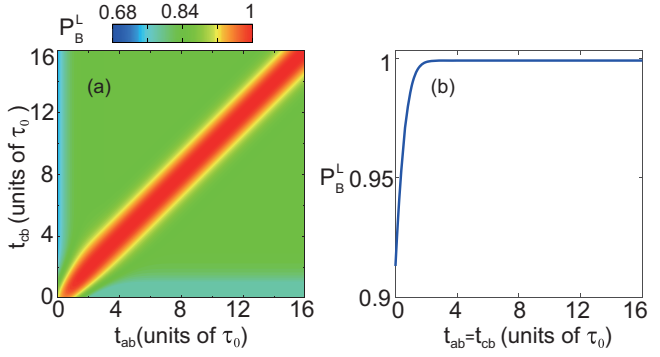

FIG. 7. Dependence of ESST on the time delays of control fields for the target state $|B\rangle$. (a) Final population of the left-handed enantiomer $P_B^L(t_f)$ versus the time delays $t_{ab} = t_a - t_b$ and $t_{cb} = t_c - t_b$. (b) Cut line plot of $P_B^L(t_f)$ along $t_{ab} = t_{cb}$.

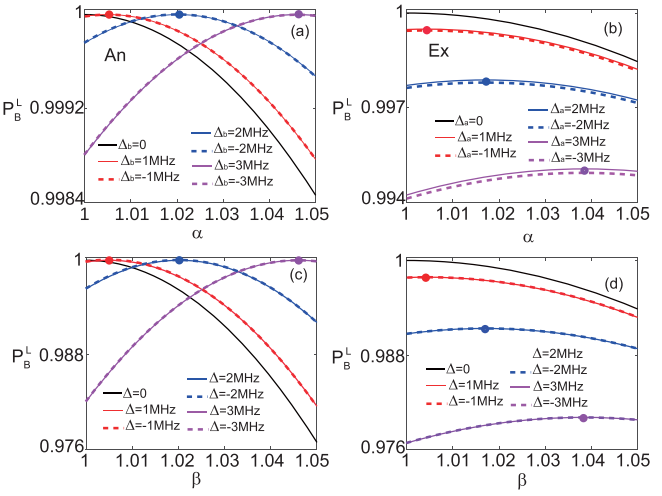

FIG. 8. Dependence of ESST on the detunings for the target state $|B\rangle$. (a) and (b) Final population $P_B^L(t_f)$ versus the scale factor α of the coupling $\Omega_b(t)$ for different values of detuning $\Delta_b = \omega_b - \omega_{AC}$. (c) and (d) Final population $P_B^L(t_f)$ versus the scale factor β of the couplings $\Omega_a(t)$ and $\Omega_c(t)$ by setting $\Delta_a = \omega_a - \omega_{AB} = \Delta_c = \omega_c - \omega_{BC} = \Delta$. The analytical simulations [(a) and (c)] are compared with the exact results [(b) and (d)].

in principle could be achieved by using the center-frequency-detuned pulses, as long as they satisfy the amplitude and phase conditions $\mathcal{E}_{a,b,c}$ and $\phi_{a,b,c}$ at transition frequencies. Figure 8 shows the dependence of $P_B^L(t_f)$ on the detunings, for which the calculated results obtained by using the analytically derived time-dependent wave functions [Figs. 8(a) and 8(c)] are compared with those from exactly numerical solutions [Figs. 8(b) and 8(d)]. We perform the simulations in Figs. 8(a) and 8(b) to calculate $P_B^L(t_f)$ for different values of $\Delta_b = \omega_b - \omega_{AC}$ while scaling the coupling $\Omega_b(t)$ with a factor α, for which the center frequencies ω_b and ω_c are fixed at the resonant conditions. The simulations in Figs. 8(c) and 8(d) are accomplished with different detunings $\Delta_a = \omega_a - \omega_{AB}$ and $\Delta_c = \omega_c - \omega_{BC}$ by scaling the couplings $\Omega_a(t)$ and $\Omega_c(t)$ with a factor β, for which we set $\Delta_a = \Delta_c = \Delta$ while setting $\Delta_b = 0$. For both analytical simulations, we can see that the detunings decrease $P_B^L(t_f)$. By increasing the strengths of the control fields, the maximal value of $P_B^L(t_f)$ can be increased to the same level as the resonant excitation, as shown in Figs. 8(a) and 8(c). For the exact simulations, however, the maximal values can be increased, but below the theoretical maximum. The differences can be attributed to the influence of high-order Magnus expansion terms, which are ignored in the analytical model. We also observe similar results for the target state $|B\rangle$ (not shown here). Thus, the center-frequency-detuned excitations with small detunings are also allowed by applying the corresponding amplitude and phase conditions at transition frequencies. The larger detunings will reduce the ESST efficiency due to the optical processes described by the higher-order (mainly second-order) terms of Magnus expansion, which strongly depend on the coupling strengths between states.

IV. CONCLUSION

We have presented a general pulse-area theorem analysis to explore ESST within a closed-loop three-level system. We considered three rotational states cyclically connected by *a*-type, *b*-type, and *c*-type components of the transition dipole molecules. Using a strategy that separates the closed-loop excitation into two stages, we derived the amplitude and phase conditions for designing three linearly polarized microwave pulses to generate ESST to different targets. The two-stage strategy we used differs from previous schemes that turned on the direct one-photon transition from the initial state to the target state before the indirect two-photon one. Our schemes first switched on one control field involved in the two-photon path by generating maximal coherent supposition between the initial and intermediate states. We examined this three-level-pulse-area theorem in cyclohexylmethanol molecules and analyzed its applications with both center-frequency-resonant and -detuned pulse sequences. For the latter, small detunings on the center frequencies of the control pulses would be expected to reduce the influence of high-order Magnus expansion terms. This introduces a fundamental question of whether one can design fast and robust quantum control schemes against center-frequency detunings. To that end, optimal and robust control methods combined with artificial intelligence algorithms could be used to search for shaped control pulses subject to multiple constraints [61,73–76].

ACKNOWLEDGMENTS

This work was supported by the National Natural Science Foundations of China under Grant No. 61973317. Y.G. was partially supported by the Scientific Research Fund of Hunan Provincial Education Department under Grant No. 20A025, Changsha Municipal Natural Science Foundation under Grant No. kq2007001, the Opening Project of Key Laboratory of Low Dimensional Quantum Structures and Quantum Control of the Ministry of Education under Grant No. QSQC1905, and the Open Research Fund of Hunan Provincial Key Laboratory of Flexible Electronic Materials Genome Engineering under Grant No. 202009.

[1] L. Pasteur, Recherches sur les relations qui peuvent exister entre la forme cristalline, la composition chimique et le sens de la polarisation rotatoire, Ann. Chim. Phys. **24**, 442 (1848).
[2] M. Quack, J. Stohner, and M. Willeke, High-resolution spectroscopic studies and theory of parity violation in chiral molecules, Annu. Rev. Phys. Chem. **59**, 741 (2008).
[3] R. Naaman and D. H. Waldeck, Spintronics and chirality: Spin selectivity in electron transport through chiral molecules, Annu. Rev. Phys. Chem. **66**, 263 (2015).
[4] R. Naaman, Y. Paltiel, and D. H. Waldeck, Chiral molecules and the electron spin, Nat. Rev. Chem. **3**, 250 (2019).
[5] M. R. Wasielewski, M. D. E. Forbes, N. L. Frank, K. Kowalski, G. D. Scholes, J. Yuen-Zhou, M. A. Baldo, D. E. Freedman, R. H. Goldsmith, T. Goodson III, M. L. Kirk, J. K. McCusker, J. P. Ogilvie, D. A. Shultz, S. Stoll, and K. B. Whaley, Exploiting chemistry and molecular systems for quantum information science, Nat. Rev. Chem. **4**, 490 (2020).
[6] C. Vogt, Separation of D/L-carnitine enantiomers by capillary electrophoresis, J. Chromatogr. A **745**, 53 (1996).
[7] R. M. Hazen and D. S. Sholl, Chiral selection on inorganic crystalline surfaces, Nat. Mater. **2**, 367 (2003).
[8] D. Patterson and M. Schnell, New studies on molecular chirality in the gas phase: enantiomer differentiation and determination of enantiomeric excess, Phys. Chem. Chem. Phys. **16**, 11114 (2014).
[9] M. F. Wahab, D. W. Armstrong, D. Roy, and C. A. Weatherly, Frontiers in ultrafast chiral chromatography, LCGC Europe **31**, 308 (2018).
[10] J. K. Jenkins, A. Salam, and T. Thirunamachandran, Retarded dispersion interaction energies between chiral molecules, Phys. Rev. A **50**, 4767 (1994).
[11] P. Barcellona, H. Safari, A. Salam, and S. Y. Buhmann, Enhanced Chiral Discriminatory van der Waals Interactions mediated by Chiral Surfaces, Phys. Rev. Lett. **118**, 193401 (2017).
[12] H. Safari, P. Barcellona, S. Y. Buhmann, and A. Salam, Medium-assisted van der Waals dispersion interactions involving chiral molecules, New J. Phys. **22**, 053049 (2020).
[13] D. P. Craig and T. Thirunamachandran, Chiral discrimination in molecular excitation transfer, J. Chem. Phys. **109**, 1259 (1998).
[14] A. Salam, Resonant transfer of excitation between two molecules using Maxwell fields, J. Chem. Phys. **122**, 044113 (2005).
[15] A. Salam, Discriminatory resonance energy transfer mediated by a third molecule, J. Phys. Chem. A **125**, 3459 (2021).
[16] J. S. Shao and P. Hänggi, Control of molecular chirality, J. Chem. Phys. **107**, 9935 (1997).
[17] G. Heppke, A. Jákli, S. Rauch, and H. Sawade, Electric-field-induced chiral separation in liquid crystals, Phys. Rev. E **60**, 5575 (1999).
[18] P. Brumer, E. Frishman, and M. Shapiro, Principles of electric-dipole-allowed optical control of molecular chirality, Phys. Rev. A **65**, 015401 (2001).
[19] K. Hoki, L. González, and Y. Fujimura, Quantum control of molecular handedness in a randomly oriented racemic mixture using three polarization components of electric fields, J. Chem. Phys. **116**, 8799 (2002).
[20] I. Thanopulos, P. Král, and M. Shapiro, Theory of a two-step enantiomeric purification of racemic mixtures by optical means: The D_2 S_2 molecule, J. Chem. Phys. **119**, 5105 (2003).
[21] E. Frishman, M. Shapiro, and P. Brumer, Optical purification of racemic mixtures by laser distillation in the presence of a dissipative bath, J. Phys. B **37**, 2811 (2004).
[22] Y. Li, C. Bruder, and C. P. Sun, Generalized Stern-Gerlach Effect for Chiral Molecules, Phys. Rev. Lett. **99**, 130403 (2007).
[23] Y. Li and C. Bruder, Dynamic method to distinguish between left- and right-handed chiral molecules, Phys. Rev. A **77**, 015403 (2008).
[24] C. Ye, Q. Zhang, and Y. Li, Real single-loop cyclic three-level configuration of chiral molecules, Phys. Rev. A **98**, 063401 (2018).
[25] C. Ye, Q. Zhang, Y. Chen, and Y. Li, Effective two-level models for highly efficient inner-state enantioseparation based on cyclic three-level systems of chiral molecules, Phys. Rev. A **100**, 043403 (2019).

[26] A. Yachmenev, J. Onvlee, E. Zak, A. Owens, and J. Küpper, Field-induced Diastereomers for Chiral Separation, Phys. Rev. Lett. **123**, 243202 (2019).

[27] J.-L. Wu, Y. Wang, J.-X. Han, C. Wang, S.-L. Su, Y. Xia, Y. Jiang, and J. Song, Two-Path Interference for Enantiomer-Selective State Transfer of Chiral Molecules, Phys. Rev. Appl. **13**, 044021 (2020).

[28] B. T. Torosov, M. Drewsen, and N. V. Vitanov, Efficient and robust chiral resolution by composite pulses, Phys. Rev. A **101**, 063401 (2020).

[29] B. T. Torosov, M. Drewsen, and N. V. Vitanov, Chiral resolution by composite Raman pulses, Phys. Rev. Research **2**, 043235 (2020).

[30] C. Ye, Q. Zhang, Y. Chen, and Y. Li, Fast Enantioconversion of chiral mixtures based on a four-level double-Δ model, Phys. Rev. Research **2**, 033064 (2020).

[31] J.-L. Wu, Y. Wang, S.-L. Su, Y. Xia, Y. Y. Jiang, and J. Song, Discrimination of enantiomers through quantum interfernce and quantum Zeno effect, Opt. Express **28**, 33475 (2020).

[32] Y. Chen, C. Ye, Q. Zhang, and Y. Li, Enantio-discrimination via light deflection effect, J. Chem. Phys. **152**, 204305 (2020).

[33] X. Xu, C. Ye, Y. Li, and A. Chen, Enantiomeric-excess determination based on nonreciprocal-transition-induced spectral-line elimination, Phys. Rev. A **102**, 033727 (2020).

[34] C. Ye, B. Liu, Y.-Y. Chen, and Y. Li, Enantio-conversion of chiral mixtures via optical pumping, Phys. Rev. A **103**, 022830 (2021).

[35] I. Tutunnikov, L. Xu, R. W. Field, K. A. Nelson, Y. Prior, and I. S. Averbukh, Enantioselective orientation of chiral molecules induced by terahertz pulses with twisted polarization, Phys. Rev. Research **3**, 013249 (2021).

[36] K. Bergmann, H. Theuer, and B. W. Shore, Coherent population transfer among quantum states of atoms and molecules, Rev. Mod. Phys. **70**, 1003 (1998).

[37] N. V. Vitanov, A. A. Rangelov, B. W. Shore, and K. Bergmann, Stimulated Raman adiabatic passage in physics, chemistry, and beyond, Rev. Mod. Phys. **89**, 015006 (2017).

[38] X. Chen, I. Lizuain, A. Ruschhaupt, D. Guéry-Odelin, and J. G. Muga, Shortcut to Adiabatic Passage in Two- and Three-Level Atoms, Phys. Rev. Lett. **105**, 123003 (2010).

[39] D. Guéry-Odelin, A. Ruschhaupt, A. Kiely, E. Torrontegui, S. Martínez-Garaot, and J. G. Muga, Shortcuts to adiabaticity: Concepts, methods, and applications, Rev. Mod. Phys. **91**, 045001 (2019).

[40] M. Shapiro, E. Frishman, and P. Brumer, Coherently Controlled Asymmetric Synthesis with Achiral Light, Phys. Rev. Lett. **84**, 1669 (2000).

[41] P. Kra'l and M. Shapiro, Cyclic Population Transfer in Quantum Systems with Broken Symmetry, Phys. Rev. Lett. **87**, 183002 (2001).

[42] P. Kra'l, I. Thanopulos, M. Shapiro, and D. Cohen, Two-step Enantio-Selective Optical Switch, Phys. Rev. Lett. **90**, 033001 (2003).

[43] D. Gerbasi, M. Shapiro, and P. Brumer, Theory of enantiomeric control in dimethylallene using achiral light, J. Chem. Phys. **115**, 5349 (2001).

[44] N. V. Vitanov and M. Drewsen, Highly Efficient Detection and Separation of Chiral Molecules Through Shortcuts to Adiabaticity, Phys. Rev. Lett. **122**, 173202 (2019).

[45] J. Wu, Y. Wang, J. Song, Y. Xia, S. Su, and Y. Jiang, Robust and highly efficient discrimination of chiral molecules through three-mode parallel paths, Phys. Rev. A **100**, 043413 (2019).

[46] E. Frishman, M. Shapiro, D. Gerbasi, and P. Brumer, Enantiomeric purification of nonpolarized racemic mixtures using coherent light, J. Chem. Phys. **119**, 7237 (2003).

[47] D. Patterson and J. M. Doyle, Sensitive Chiral Analysis via Microwave Three-Wave Mixing, Phys. Rev. Lett. **111**, 023008 (2013).

[48] D. Patterson, M. Schnell, and J. M. Doyle, Enantiomer-specific detection of chiral molecules via microwave spectroscopy, Nature (London) **497**, 475 (2013).

[49] V. A. Shubert, D. Schmitz, D. Patterson, J. M. Doyle, and M. Schnell, Identifying enantiomers in mixtures of chiral molecules with broadband microwave spectroscopy, Angew. Chem. Int. Ed. **53**, 1152 (2014).

[50] V. A. Shubert, D. Schmitz, C. Medcraft, A. Krin, D. Patterson, J. M. Doyle, and M. Schnell, Rotational spectroscopy and three-wave mixing of 4-carvomenthenol: A technical guide to measuring chirality in the microwave regime, J. Chem. Phys. **142**, 214201 (2015).

[51] S. Lobsiger, C. Pérez, L. Evangelisti, K. K. Lehmann, and B. H. Pate, Molecular structure and chirality detection by Fourier transform microwave spectroscopy, J. Phys. Chem. Lett. **6**, 196 (2015).

[52] S. Eibenberger, J. Doyle, and D. Patterson, Enantiomer-Specific State Transfer of Chiral Molecules, Phys. Rev. Lett. **118**, 123002 (2017).

[53] S. R. Domingos, C. Perez, and M. Schnell, Sensing chirality with rotational spectroscopy, Annu. Rev. Phys. Chem. **69**, 499 (2018).

[54] C. Pérez, A. L. Steber, A. Krin, and M. Schnell, Statespecific enrichment of chiral conformers with microwave spectroscopy, J. Phys. Chem. Lett. **9**, 4539 (2018).

[55] M. Leibscher, T. F. Giesen, and C. P. Koch, Principles of enantio-selective excitation in three-wave mixing spectroscopy of chiral molecules, J. Chem. Phys. **151**, 014302 (2019).

[56] A. Bambini and P. R. Berman, Analytic solutions to the two-state problem for a class of coupling potentials. Phys. Rev. A **23**, 2496 (1981).

[57] G. F. Thomas, Validity of the Rosen-Zener conjecture for Gaussian-modulated pulses, Phys. Rev. A **27**, 2744 (1983).

[58] D. Sugny and C. Kontz, Optimal control of a three-level quantum system by laser fields plus von Neumann measurements, Phys. Rev. A **77**, 063420 (2008).

[59] Y. Guo, L. Zhou, L. M. Kuang, and C. P. Sun, Magneto-optical Stern-Gerlach effect in an atomic ensemble, Phys. Rev. A **78**, 013833 (2008).

[60] G. Shchedrin, C. O'Brien, Y. Rostovtsev, and M. O. Scully, Analytic solution and pulse area theorem for three-level atoms, Phys. Rev. A **92**, 063815 (2015).

[61] Y. Guo, X. B. Luo, S. Ma, and C.-C. Shu, All-optical generation of quantum entangled state with strict constrained ultrafast laser pulses, Phys. Rev. A **100**, 023409 (2019).

[62] B. Y. Chang, I. R. Sola, and V. S. Malinovsky, Anomalous Rabi Oscillations in Multilevel Quantum Systems, Phys. Rev. Lett. **120**, 133201 (2018).

[63] H. Mineo, G.-S. Kim, S. H. Lin, and Y. Fujimura, Dynamic stark-induced coherent π-electron rotations in a chiral aromatic

ring molecule: Application to phenylalanine, J. Phys. Chem. A **123**, 6399 (2019).

[64] Y Guo, C.-C. Shu, D. Y. Dong, and F. Nori, Vanishing and Revival of Resonance Raman Scattering, Phys. Rev. Lett. **123**, 223202 (2019).

[65] C.-C. Shu, Q.-Q. Hong, Y. Guo, and N. E. Henriksen, Orientational quantum revivals induced by a single-cycle terahertz pulse, Phys. Rev. A **102**, 063124 (2020).

[66] C.-C. Shu, Y. Guo, K.-J. Yuan, D. Y. Dong, and A. D. Bandrauk, Attosecond all-optical control and visualization of quantum interference between degenerate magnetic states by circularly polarized pulses, Opt. Lett. **45**, 960 (2020).

[67] Q.-Q. Hong, L.-B. Fan, C.-C. Shu, and N. E. Henriksen, Generation of maximal three-state field-free molecular orientation with terahertz pulses, Phys. Rev. A **104**, 013108 (2021).

[68] A. Salam and W. J. Meath, On the control of excited state relative populations of enantiomers using circularly polarized pulses of varying durations, J. Chem. Phys. **106**, 7865 (1997).

[69] A. Salam and W. J. Meath, On enantiomeric excesses obtained from racemic mixtures by using circularly polarized pulsed lasers of varying durations, Chem. Phys. **228**, 115 (1998).

[70] Y. Ma and A. Salam, On chiral selectivity of enantiomers using a circularly polarized pulsed laser under resonant and off-resonant conditions, Chem. Phys. **324**, 367 (2006).

[71] K. K. Lehmann, Influence of spatial degeneracy on rotational spectroscopy: Three-wave mixing and enantiomeric state separation of chiral molecules, J. Chem. Phys. **149**, 094201 (2018).

[72] S. Blanes, F. Casas, J. A. Oteo, and J. Ros, The Magnus expansion and some of its applications, Phys. Rep. **470**, 151 (2009).

[73] C.-C. Shu, T.-S. Ho, X. Xing, and H. Rabitz, Frequency domain quantum optimal control under multiple constraints, Phys. Rev. A **93**, 033417 (2016).

[74] Y. Guo, D. Dong, and C.-C. Shu, Optimal and robust control of quantum state transfer by shaping spectral phase of ultrafast laser pulses, Phys. Chem. Chem. Phys. **20**, 9498 (2018).

[75] D. Dong, C.-C. Shu, J. C. Chen, X. Xing, H. L. Ma, Y. Guo, and H. Rabitz, Learning control of quantum systems using frequency-domain optimization algorithms, IEEE Trans. Control. Syst. Technol. **29**, 1791 (2021).

[76] X. W. Liu, G. J. Zhang, J. Li, G. L. Shi, M. Y. Zhou, B. Q. Huang, Y. J. Tang, X. H. Song, and W. F. Yang, Deep Learning for Feynman's Path Integral in Strong-Field Time-Dependent Dynamics, Phys. Rev. Lett. **124**, 113202 (2020).